ISSN 0023-1584, Kinetics and Catalysis, 2011, Vol. 52, No. 1, pp. 62–71. © Pleiades Publishing, Ltd., 2011.

Kinetics and Mechanism of the Reaction of Novel Low Spin Fe(II)–Azo Amino Acid Complexes with Hydrogen Peroxide in Aqueous Solutions and in Aqua–Methanol Binary Mixtures[1]

A. M. Shaker, F. M. El-Cheikh, and M. S. S. Adam

Chemistry Department, Faculty of Science, Sohag University, Sohag 82524, Egypt

e-mail: adam_moamed@lycos.com

Received August 8, 2009

Abstract—Kinetics of Fe(II)–azo complexes derived from amino acids (DL-phenylalanine, DL-tryptophane, histidine and alanine) and *p*-nitroso aromatic substituted amines (*N*,*N*-dimethylamino-4-nitrosoaniline and *N*,*N*- dimethylamino-4-nitrosoaniline) with hydrogen peroxide in the aqueous solutions and under pseudo-first order conditions have been studied. The reaction exhibits two-stage kinetics. The reaction mechanism was proposed and discussed in terms of complex structure, pH and nature of the medium. The activation parameters and pK_a values were evaluated and correlated with the structural effects of the complexes.

DOI: 10.1134/S0023158411010162

Azo compounds constitute an important class of industrial, medical and biological interests. Azo amino acids are used as dyes in polish, soap, cooking oils and margarine. For these reasons, novel azo amino acid compounds were synthesized and chelated to low valent Fe(II) ions.

In literatures, kinetics of reactions of Fe(II) complexes of different ligands with H_2O_2 (Fenton's Reactions) were discussed in details [1–6]. Rate laws for those reactions of Fe(II) complexes have been discussed in terms of ion-pair or parallel dissociation and oxidation [7, 8], as well as, simple bimolecular oxidation with appropriate contribution from radicals generated during the reaction. Thus, the observed rate constants of these reactions are composite with terms corresponding to the rate-determining dissociation and the rate-determining oxidation [9, 10].

Moreover, many studies discussed kinetics of the reactions of azo compounds, particularly azo dyes [11] with H_2O_2 for the importance of these studies industrially [12, 13], environmentally [14] and biologically [15]. Detailed kinetic and spectroscopic investigations have been made on the oxidation of 4-(4-sulphonylazo)-1-naphthol, 4-(1-sulphonylazo)-2-naphthol and series of substituted 1-arylazo-2-naphthol dyes by hypochlorite, peracids and H_2O_2 in aqueous media [16] and in different pH [17]. It is so far for in literatures the kinetic studies of the reaction of Fe(II)–azo complexes with peroxo reagents generally and H_2O_2 specifically.

The applicability of the current study in the environmental aspects would be the possibility of recovery of hazardous colored azo dyes and their chelates produced from textile fibers, and from waste water by using suitable and cheap oxidants viz. H_2O_2. The final products like H_2O, O_2 or CO_2 are environmentally friendly. Therefore, we managed to discuss kinetics of the reaction between some novel low spin Fe(II)–azo complexes and H_2O_2 (see scheme 1).

EXPERIMENTAL

Materials

All chemicals used in the preparation of the complexes and in the kinetics are tafr1 of analytical grade AnalaR reagent (BDH and Aldrich) products.

The studied complexes and their corresponding ligands were synthesized and characterized by Shaker et al. (Scheme 1) [18]. The purity of the complex was tested spectrophotometrically (Fig. 1) [18] and by confirming that the kinetics were exactly first-order over the first 2.5 half lives and that the measured rate constants agreed with the literature values [18–20], Moreover, the formation of these complexes was confirmed by potentiometric titration in nitric acid with constant ionic strength $I = 0.1$ mol dm^{-3} using KNO_3, cf. Fig. 2. As shown, the tested complex begins forming at pH ≈ 3.

Kinetic Measurements

The recent kinetic measurements were executed under pseudo-first order conditions. H_2O_2 was mixed in a large excess (0.1 to 2.0 mol dm^{-3}) over the complex (1×10^{-4} mol dm^{-3}) at constant ionic strength

[1] The article is published in the original.

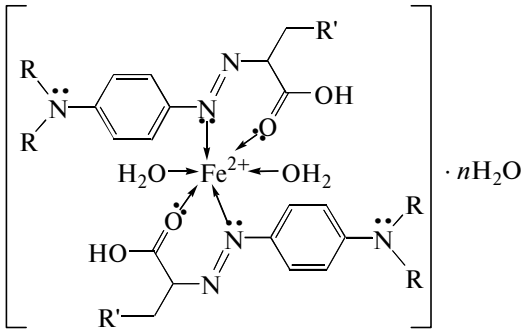

Ligand	Complex abbr.	R'	R	X	*n*
[Diaqua di(2-{[4-(dimethylamino)phenyl]azo}-3-phenylpropanoic acid) ferrous] sulphate	MphA	Ph	CH_3	SO_4	2
[Diaqua di(2-{[4-(diethylamino)phenyl]azo}-3-phenylpropanoic acid) ferrous] sulphate	EphA	Ph	C_2H_5	SO_4	3
[Diaqua di(2-{[4-(dimethylamino)phenyl]azo}-3-indol-3-ylpropanoic acid) ferrous] sulphate	MinA	indolyl	CH_3	SO_4	3
[Diaqua di(2-{[4-(diethylamino)phenyl]azo}-3-indol-3-ylpropanoic acid) ferrous] sulphate	EinA	indolyl	C_2H_5	SO_4	2
[Diaqua di(2-{[4-(dimethylamino)phenyl]azo}-3-imidazol-3-ylpropanoic acid) ferrous] sulphate	MimA	imida-zolyl	CH_3	SO_4	3
[Diaqua di(2-{[4-(diethylamino)phenyl]azo}-3-imidazol-3-ylpropanoic acid) ferrous] chloride	EimA	imida-zolyl	C_2H_5	2Cl	5
[Diaqua di(2-{[4-(diethylamino)phenyl] azo}propanoic acid) ferrous] chloride	EprA	methyl	C_2H_5	2Cl	4

Scheme 1. The chemical structure of Fe(II)-azo complexes.

(0.1 mol dm^{-3}) of KNO_3, pH ≈ (1.8–2.3), the stability range of the complexes [18] at 298 K. The reaction kinetics were followed by monitoring the decrease in absorbance A at $\lambda_{max} = 485–500$ nm of each complex, over the first 2.5 half lives for each run [20]. Observed first-order rate constants were computed by least-squares from the slopes of the plots (ln A vs. time, t), cf. Fig. 3. Repeated spectral scans were recorded for the reactions of different molar ratios of complex to H_2O_2 (1 : 1, 1 : 30, and 1 : 3000), respectively, as representative work, to get more kinetic evidences for the studied reaction mechanism, cf. Figs. 4, 5.

RESULTS AND DISCUSSION

All complexes showed two-stage kinetics, cf. Fig. 3. Standard kinetic analyses of these plots gave good estimates for the observed rate constants of the fast and slow stages. The first stage corresponds to the parallel attack reactivities of H_2O_2 on more labile *fac* (first stage) and inert *mer* (second stage) isomers of the complexes (Fig. 3, Scheme 2). Similar isomer observations were detected and analyzed kinetically in elsewhere reports [21, 22].

The contribution from the labile isomer in the reactivity of the reaction readily becomes minor at 10–15% of the time elapsed for the total kinetic run, cf. Fig. 3. Thus, the observed first-order rate constants k_{obs} were evaluated from the slopes of the slow second stage (Fig. 3, Table 1). The plots of k_{obs} vs.

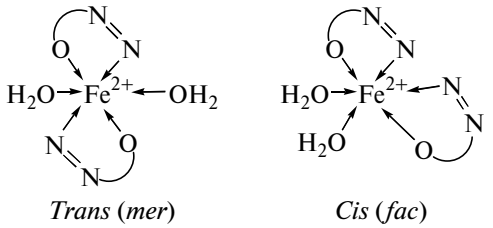

Trans (*mer*) *Cis* (*fac*)

Scheme 2. The two isomeric structures of Fe(II)–azo complexes.

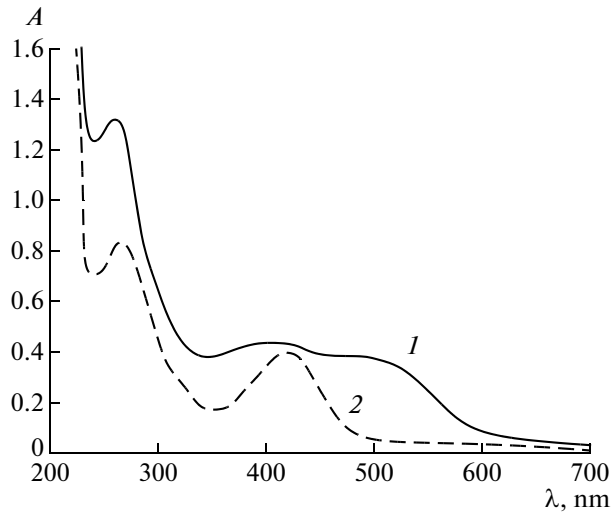

Fig. 1. Molecular electronic spectra of MphA and its corresponding ligand in the aqueous solutions and methanolic solutions, respectively, at [complex] and [ligand] = 1×10^{-4} mol dm^{-3} and 298 K. *1*—The MphA complex, *2*—the MphA ligand.

$[H_2O_2]$ exhibited linear relation with the rate law in Eq. (1).

$$-\mathrm{d[complex]}/\mathrm{d}t = k_{obs}[\mathrm{complex}]. \quad (1)$$

The spectra of Fe(II)–azo complexes show three main peaks at 250–270, 360–420, and 480–500 nm corresponding to $\pi\,\pi^*$, M-LCT and *d-d* transitions in these complexes [18]. Injection of H_2O_2 in the complex solution enhances the molar absorptivities of the bands at 500 and 270 nm to maximum values with slight shift, then decay, cf. Fig. 4. The enhancement of these bands was explained elsewhere as due to the formation of intraperoxo-intermediate [23–25]. It is assumed that the 360–420 nm bands in the original complexes decay and add to the bands at 480–500 nm during the formation of the peroxo-intermediate. In other words, the intermediate has two bands at 250–270 and 480–500 nm in common with the complexes employed. The rate and the extent of the enhancement depend on the [complex] : $[H_2O_2]$ ratio. This means that, in equimolar ratio, the growth occurs slowly, cf. Fig. 4, and the intermediate complexes have not decomposed within 24 h due to low concentration of H_2O_2. Unfortunately, several trails have been made to isolate the peroxo-intermediate, but faced with failure. The slow formation of intermediates was observed only in equimolar solutions, ca. 1×10^{-4} mol dm^{-3}. This result would be understood if the slow decomposition of the peroxo-intermediate, in parallel with its second-order formation kinetics, has been taken into consideration, particularly when measurable mass of this intermediate is formed. Furthermore, it is proba-

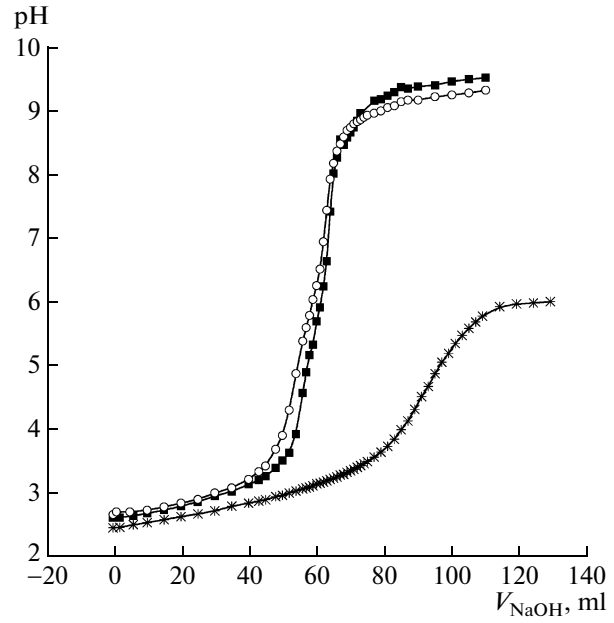

Fig. 2. Potentiometric titration curves for HNO_3 (0.01 mol dm^{-3}), HNO_3 (0.01 mol dm^{-3}) + MinA ligand (10^{-3} mol dm^{-3}) and HNO_3 (0.01 mol dm^{-3}) + MinA ligand (10^{-3} mol dm^{-3}) + MinA complex (10^{-3} mol dm^{-3}) vs. NaOH (10^{-5} mol dm^{-3}) in the aqueous solutions at 298 K. ■ HNO_3, ○ HNO_3 + MinA ligand, ∗ HNO_3 + MinA ligand + Fe^{2+}.

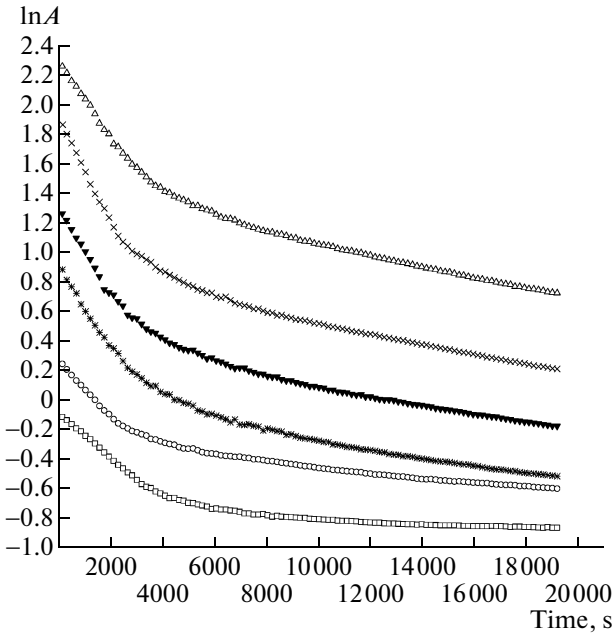

Fig. 3. The observed first-order rate plots for the reaction of MinA with $[H_2O_2]$ in the aqueous solutions, at [MinA] = 1×10^{-4} mol dm^{-3}, I = 0.10 mol dm^{-3}, pH 2 and 298 K (λ_{max} = 498 nm). △—0.1 M H_2O_2 (ln A + 1.5), ×—0.3 M H_2O_2 (ln A + 1.0), ▼—1.0 M H_2O_2 (ln A + 0.5), ∗—1.2 M H_2O_2, ○—1.8 M H_2O_2 (ln A – 0.5), □—2.0 M H_2O_2 (ln A – 1.0).

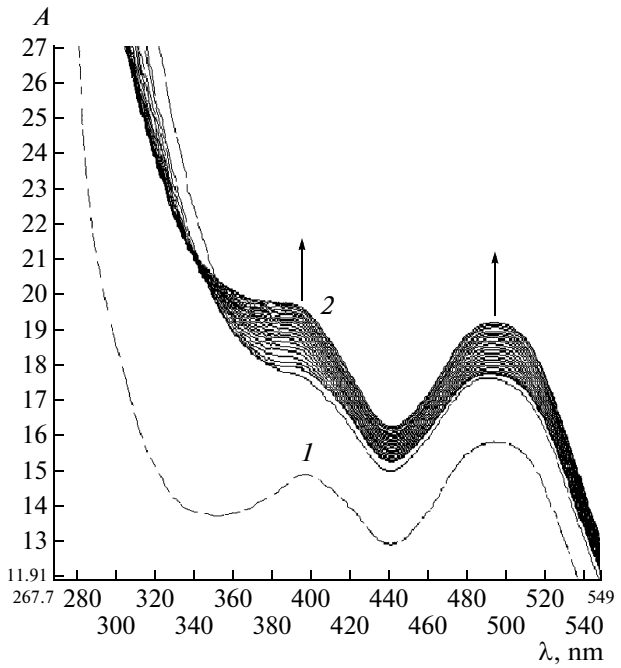

Fig. 4. Repeated molecular electronic spectral scans during the reaction of MimA with H_2O_2 in an equimolar aqueous solution of 1×10^{-4} mol dm^{-3} each with interval time 20 min (for ~4 h), at $I = 0.10$ mol dm^{-3}, pH 2 and 298 K. (For the slow rate of formation ↑ of the peroxo-intermediate complex, the decomposition has not yet been detected within 24 h.) *1*—The MphA complex before addition of H_2O_2, *2*—the MphA complex after addition of H_2O_2 (1×10^{-4} M).

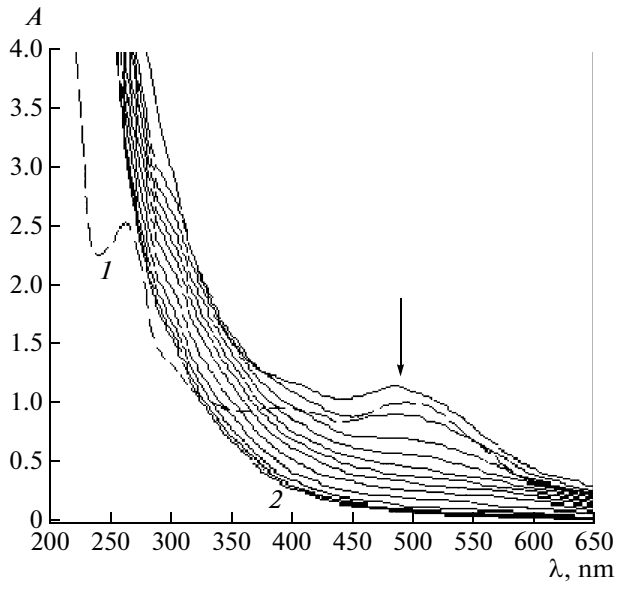

Fig. 5. Repeated molecular electronic spectral scans during the reaction of MimA with H_2O_2 in an aqueous solution (containing 1 : 3000 molar ratio of complex : H_2O_2) with interval time 20 min (for ~4 h), at [complex] = 1×10^{-4} mol dm^{-3}, [H_2O_2] = 0.30 M, $I = 0.10$ mol dm^{-3}, pH 2 and 298 K. (For the very fast rate of formation ↑ and the slow decomposition ↓ of the peroxo-intermediate complex.) *1*—The MimA complex before addition of H_2O_2, *2*—the MimA complex after addition of H_2O_2 (0.30 M).

bly that an ion-pair intermediate between the cation complex and peroxide forms in the equimolar reaction mixture employed in the kinetic test. In the presence of 1 : 30 molar ratio of [complex] : [H_2O_2] the growth renders faster and to a least extent prior to the decay. Upon mixing very large excess of H_2O_2, i.e., in 1 : 3000 molar ratio, the rate of the band growth renders too rapid to follow by conventionally available spectrophotometric tools, cf. Fig. 5. A slight enhancement of the band at 500 nm was observed just after mixing the complex solution with H_2O_2, then decays.

Therefore, a kinetic investigation has been made for the slow growth of the band at 500 nm, cf. Fig. 4, corresponding to the formation of the intraperoxo-

Table 1. The observed first-order rate constant values k_{obs} for the reaction of Fe(II)–azo complexes with H_2O_2 in the aqueous media, at [complex] = 1×10^{-4} mol dm^{-3}, $I = 0.1$ mol dm^{-3}, pH 2 and 298 K

[H_2O_2], mol dm^{-3}	$k_{obs} \times 10^4$, s^{-1}						
	MphA	EphA	MinA	EinA	MimA	EimA	EprA
0.1	0.73				1.16	0.25	
0.3	1.49	1.00	0.93	0.97	1.77	0.84	0.96
0.8	1.86	2.28	1.90		2.35		2.37
1.0			2.76	2.16		2.67	
1.2		2.42		2.65	3.27	2.97	2.81
1.4	3.15	3.00	2.77	2.99	3.19	3.31	3.13
1.8	3.57	3.80	3.64		3.82		3.79
2.0	4.21	4.04		3.80		4.19	4.08

Table 2. The values of the component rate constant values as calculated by least squares of the plots of k_{obs} vs. $[H_2O_2]$ of Fe(II)–azo complexes in the aqueous media, at [complex] = 1×10^{-4} mol dm^{-3}, $I = 0.1$ mol dm^{-3}, pH 2 and 298 K

Complexe	$k_1 \times 10^5$, s^{-1}	$k_2 \times 10^4$, mol^{-1} dm^3 s^{-1}
MphA	7.03	1.68
EphA	5.83	1.74
MinA	5.74	1.73
EinA	5.20	1.69
MimA	1.18	1.52
EimA	2.52	2.12
EprA	6.66	1.75

complex intermediate in the equimolar ratios. So, a linear second-order plots ($1/A$ vs. t) were obtained for the formation of the intermediate complex. Absorbance, A, displayed in these plots is given by

$$A = (A_{max} - A_0) - (A_t - A_0), \quad (2)$$

where A_{max} is the maximum absorbance value at 500 nm in Fig. 4, A_0 is the minimum absorbance and A_t is the absorbance at any arbitrary time. Therefore, the second-order kinetics plotted is given as

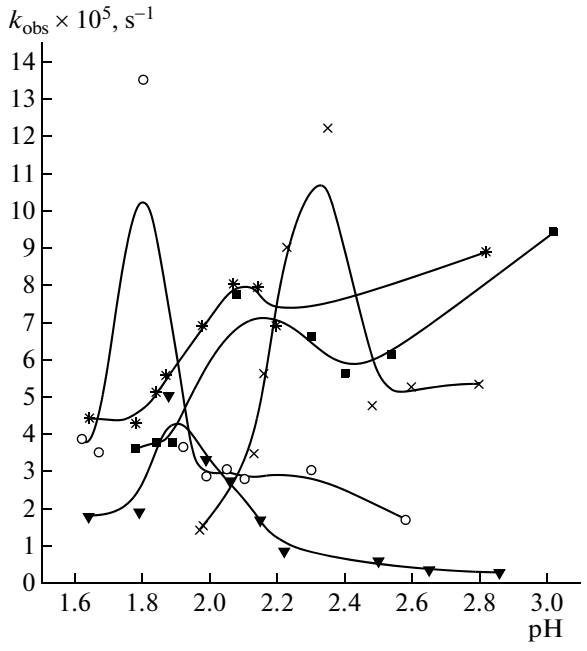

Fig. 6. Plot of the observed first-order rate constants of EphA, MinA, EinA, MimA, and EprA vs. pH of the stability range in the aqueous solutions, at [complex] = 1×10^{-4} mol dm^{-3}, $[H_2O_2] = 0.30$ M, $I = 0.10$ mol dm^{-3} and 298 K. ■—EphA, ○—MinA, ▼—EinA, *—MimA, ×—EprA.

$$\frac{1}{(A_{max} - A_0) - (A_t - A_0)} = \frac{k_2 t}{\Delta\varepsilon L} + \frac{1}{(A_{max} - A_0)} \quad (3)$$

and the rate law can be assumed as

$$\frac{d[Int]}{dt} = \frac{-d[complex]}{dt} = k_2[complex][H_2O_2], \quad (4)$$

where Int is the intermediate. This is providing that, the decomposition of the intermediate is negligible, especially in the earlier stages of the reaction. This kinetic behavior probably points to the development of peroxo-intermediates via substitution of one H_2O_2 molecule and/or peroxo anion for one of the two coordinated H_2O molecules (Scheme 1).

The studied growth of the peroxo-intermediate follows pseudo-first order kinetics, in the presence of large excess of $[H_2O]$ compared to [complex], i.e., in (1 : 30) or (1 : 3000) molar ratios, which is very fast. The rate of decay of the parent complex is approximately the same as that rate of the decay of the intermediate leading to the final products. The rate law can be assumed as

$$\frac{-d[complex]}{dt} = \frac{-d[complex\text{-}Int]}{dt} = \frac{d[P]}{dt} = k_{obs}[complex], \quad (5)$$

where P is the final product, and the observed rate constant k_{obs} follows the relation:

$$k_{obs} = k_1 + k_2[H_2O_2]. \quad (6)$$

Again, this indicates the formation of *mono*-peroxo complex intermediate. k_1 corresponds to the rate constant of aquation of the azo complex in the pH range 1.8–2.3 used in all kinetic runs. The plots of k_{obs} vs. $[H_2O_2]$ present linear relations with intercept values of k_1 and slopes values of k_2 from least squares of these plots, cf. Table 2, indicating direct attack of H_2O_2 on the complex in the reaction.

In acidic solutions, pH ≤ 4, where our complexes exhibit their high stability and these are the media of following kinetics of all runs with almost 20% aquation of the initial concentration of the complex in the reaction mixture in an average time of a month. In the solutions of pH range ~1.8–2.3 the complexes keep their intensely reddish violet color within the reported time.

Figure 6 shows reactivity profiles with pH within the stability range values of the studied complexes. These profiles show reactivity peaks at pHs 1.5–3. In this pH range, isosbestic points were established at 395 and 446 nm [18] due to the existence of the equilibrium between azo (ammonium form) and azonium forms. The intensification of the reddish violet color of our complexes in these pH media may be an evidence for the establishment of this equilibrium. The protonation equilibrium and this type of pH profiles were observed before by Beck [26]. The reactivity peaks

Table 3. Second-order rate constant values k_2 and the activation parameters for the reaction of EphA, EimA, EinA and EprA with H_2O_2 at different temperatures, at [complex] = 1×10^{-4} mol dm^{-3}; [H_2O_2] = 0.30 M, I = 0.1 mol dm^{-3} and pH 2

Complex	Temperature, K				E_a kJ M^{-1}	$\Delta H^{\neq}$ J M^{-1}	$\Delta G^{\neq}$ kJ M^{-1}	$\Delta S^{\neq}$ J M^{-1} K^{-1}	A M^{-1} s^{-1}
	288	293	303	308					
EinA	0.83	0.90	0.96	1.01	112.9	36.39	23.01	−77.08	2.63
EphA	0.87	0.94	0.99	1.08	60.08	38.04	72.7	−24.26	5.12
EimA	0.93	0.97	1.04	1.16	68.47	37.73	9.76	−32.65	6.91
EprA	1.01	1.02	1.10	1.27	97.80	37.03	18.51	−61.98	13.94

Note: $k_2 \times 10^4$, mol^{-1} dm^3 s^{-1}.

locate at pH starting from 1.8 for MinA with the less donor *N*,*N*-dimethyl substituent to the phenyl moiety and the most electron-attracting indolyl attached to the amino acid moiety and ending at 2.3 for EprA with two donor groups on both sides, the more donor *p*-*N*,*N*-diethyl on the phenyl side and $-CH_3$ group on the amino acid opposite side. These reactivity peaks were assumed to be due to the full protonation of *N*,*N*-dialkylamino whereby retarding the intramolecular *CT* within the complex and enhancing the reactivity towards the attack of H_2O_2.

The observed decrease in k_{obs} at pH ≤ 2 is probably attributed to the full protonation of the azo ligand leading to reduce the basicity and then the reactivity towards H_2O_2 reagent. Furthermore, in these strong acid media, H_2O_2 exists in its conjugate acid form with low nucleophilicity.

At higher pH ≥ 4, the azo ligands in the complexes fully deprotonate, and the azonium (Schiff base) tautomer prevails. Schiff base tautomers exhibit high reactivities against aquation and base hydrolysis, cf. Scheme 3.

The shift in λ_{max} from 390 to 500 nm or equivalently, the decay of the band at 390 nm and its growth on $d \longrightarrow d$ transition band at 500 nm, enhances the latter band and renders broad (Figs. 4 and 5). This evidence, and the development of the absorption peak at 270 nm. are comparable with those observations reported for Fe(II)edta–H_2O_2 [27, 28]. The high negative entropies of activation assume an experimental evidence against the release of carboxylate in the azo ligand by peroxide, cf. Table 3, the second pathway suggested by Francis et al. [29] for the reaction of H_2O_2 with Fe(II)edta-(ethylenediamine-tetraacetate)$^{4-}$.

The reaction studied, in this work, implies the following disproportionation of H_2O_2

$$2H_2O_2 \longrightarrow 2H_2O + O_2, \qquad (I)$$

catalyzed by the Fe(II)–azo complexes, as well as, the break down of the oxidized complexes, Fe(III)- azo chelates. Our complexes undergo catalysis due to the ability of Fe to form two oxidation states, Fe(II) and Fe(III), and the structure of the present metal complexes containing labile replaceable coordinated ligands, mainly H_2O molecules.

An interesting observation, in the recent investigation, is the possibility of spectroscopically visible growth of the peroxo-Fe(II)–azo intermediate complex as mentioned above, cf. Fig. 4. The formation of the peroxo-intermediate follows pseudo-first order kinetics in the mixing molar ratio 1 : 30 [complex] : [H_2O_2]. In equimolar ratio, the peroxo-substitution reaction follows second-order kinetics, first-order in each of [complex] and [H_2O_2]. This kinetic evidence probably supports the mechanism that only one peroxo ion replaces one coordinated H_2O. In literatures [23–25, 28], the growth of bands at 270 and 500 nm and decay of band at 390 nm suggest the formation of new Fe(II) species, namely peroxo-intermediates. A further support for the mechanism is the visual color changes just after addition of H_2O_2 to the complex from reddish violet ⟶ more intense reddish violet ⟶ pale reddish violet ⟶ violet ⟶ pale violet ⟶ pale brown ⟶

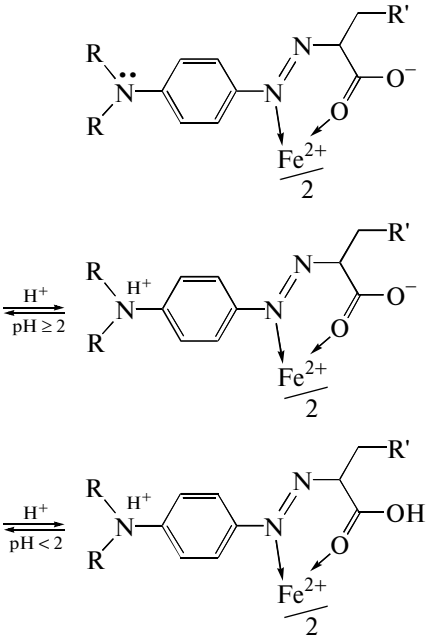

Scheme 3.

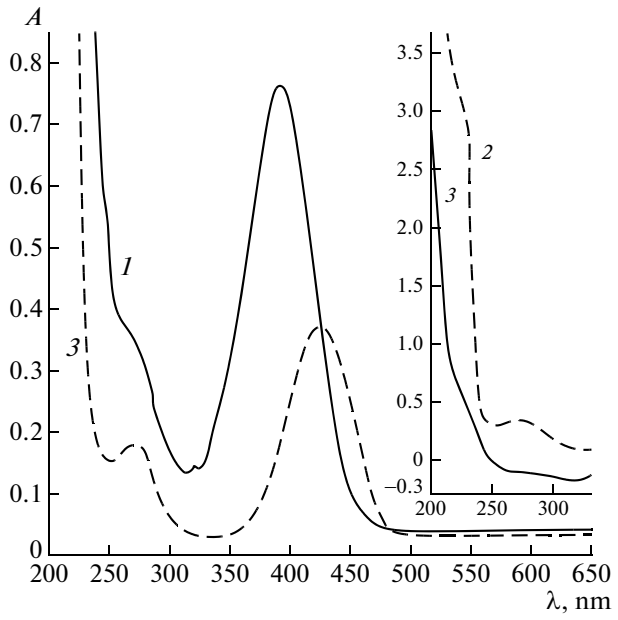

Fig. 7. A comparison of spectral scans of the products of the reaction between MimA and H_2O_2 with *N*,*N*-dimethylamino-4-nitrosoaniline and histidine as reagents for the formation of MimA. *1*—*p*-Nitroso-*N*,*N*-dimethylaniline, *2*—histadine, *3*—the product.

yellow to finally pale yellow. The more intensive color probably assumes the substitution of H_2O_2 and/or peroxo in the place of coordinated H_2O. Fading in color supports oxidation followed by decomposition of the complex.

The final product from both oxidation and decomposition of our chelates were characterized. The absorption spectra of the final products were consistent with these spectra of the reference samples of the corresponding free amino acid (histidine, λ_{max} = 275 nm) and *N*,*N*-dialkylamino-*p*-nitroaniline, λ_{max} = 385 nm, cf. Fig. 7. The solid line spectra correspond to the final product (*p*-nitro-*N*,*N*-dimethylaniline (λ_{max} = 385 nm), but the dashed line spectra are for *p*-nitroso-*N*,*N*-dimethylaniline (λ_{max} = 420 nm). The brown precipitate formed, long after the end of each kinetic run, settling down in the spectrophotometric cell, indicates the formation of the nitro derivative, the oxidation product of *N*,*N*-dimethyl-*p*-nitrosoaniline. In the same Figure, the spectral dotted line is for a reference amino acid (histidine) and solid line spectra for amino acid product from the reaction. The brown precipitate disappears long after the end of the kinetic reaction (2–3 days), presumably due to the coordination of Fe^{3+} ions to the nitro product with disappearance of the band at 385 nm. The pale yellow color formed at the end of each kinetic run indicates the formation of Fe^{3+} ions which gave red color with thiocyanate test.

The reaction exhibits a mechanism in which a composite rate-limiting step is assumed as substitution and oxidation in equimolar reaction mixtures and in the presence of excessive molar ratios of H_2O_2 up to 30 fold the concentration of the complex, as shown below.

$$\underset{\text{A}}{[\text{Fe(II)L}_2(\text{H}_2\text{O})_2] + 2\text{H}^+} \quad \text{(II)}$$
$$\rightleftharpoons^{K_1} \underset{\text{A}^{2+}}{[\text{Fe(II)(HL)}_2(\text{H}_2\text{O})_2]^{2+}},$$

$$\text{H}_2\text{O}_2 \rightleftharpoons^{K_1} \text{HOO}^- + \text{H}^+, \quad \text{(III)}$$
$$K_2 = 5.59 \times 10^{-12}\ \text{mol dm}^{-3},$$

$$\underset{\text{A}^{2+}}{[\text{Fe(II)(HL)}_2(\text{H}_2\text{O})_2]^{2+}} + \text{H}_2\text{O}_2 \quad \text{(IV)}$$
$$\xrightarrow[\text{slow}]{k_4} \underset{\text{B}^+}{[\text{Fe(II)(HL)}_2(\text{H}_2\text{O})(\text{HOO})]^+} + \text{H}_2\text{O} + \text{H}^+,$$

$$\overset{\text{e}^-}{\underset{\text{B}^+}{[\text{Fe(II)(HL)}_2(\text{H}_2\text{O})(\text{HOO})]^+}} \quad \text{(V)}$$
$$\xrightarrow[\text{slow}]{k_4} \underset{\text{C}^+}{[\text{Fe(III)(HL)}_2(\text{H}_2\text{O})(\text{O})]^+} + \text{HO}^\bullet,$$

$$\underset{\text{C}^+}{[\text{Fe(III)(HL)}_2(\text{H}_2\text{O})(\text{O})]^+} + 2\text{HO}^\bullet + 2\text{H}_2\text{O}_2 + 4\text{H}^+ \quad \text{(VI)}$$
$$\xrightarrow[\text{fast}]{k_5} \text{Fe}^{3+} + 2(\text{R}')_2\text{NHPhNO}_2 + 2\text{RCH}_2\text{CH(NH}_2\text{)COOH} + 4\text{H}_2\text{O},$$

where $HL^+ = R'_2N^+H{-}Ph{-}N{=}N{-}CH(COOH)CH_2R$, K_1 is the protonation constant value of the complex [18].

The decomposition of the complex after oxidation *via* inner-sphere electron transfer is assumed to be due to that the smaller Fe^{3+} ionic size no longer so fits the ligand cavity as to the larger size Fe^{2+} ion. As mentioned elsewhere [30], that the mechanism for the decoloration of azo dyes with hydrogen peroxide is not quite understood, but assumed as hydroxyl radicals attacking the organic colorants and destroying the chromophore, azo group (N=N). Hydroxyl free radical adds to the azo chromophore and homocleaves it. Excess hydrogen peroxide in the reaction, oxidizes *N*,*N*-dialkylamino-*p*-nitrosoaniline to the corresponding *p*-nitro derivative. The presence of free radicals in the reaction mechanism was tested by the addition of acrylonitrile and the formation of white gel precipitate after a period from the beginning of the kinetic run [31].

In the presence of very large excess of H_2O_2 (0.30 M), the substitution reaction (IV) in the mechanism proposal, is assumed to be fast. Assuming the steady state approximation for the intermediates B^+ and C^+ and setting $[A]_T$ as

$$[A]_T = [A^{2+}] + [B^+], \quad (7)$$

where $[A]_T$ is the total analytical concentration of the complex.

This is provided that $[C^+]_{ss} \approx 0$ due to its much higher reactivity. Thus, the following rate equation can be formulated as follows

$$\frac{-d[complex]}{dt} = K_1k_3(1 + k_4)[A]_T[H^+][H_2O_2]. \quad (8)$$

In the presence of very large excess of $[H_2O_2]$ and $[H^+]$ compared to $[A]_T$, thus the rate law becomes

$$\frac{-d[complex]}{dt} = k_{obs}[A]_T. \quad (9)$$

Accordingly, on comparing Eqs. (8) and (9), k_{obs} can be deduced as

$$k_{obs} = K_1k_3(1 + k_4)[H^+][H_2O_2], \quad (10)$$

$$[H_2O_2]_T = [H_2O_2] + [HOO^-] + [B^+] + [C^+], \quad (11)$$

where $[H_2O_2]_T$ is the total analytical concentration of hydrogen peroxide.

Assuming that, $[B^+] = [C^+] \approx 0$, due to their high reactivity, particularly in the presence of very large excess of $[H_2O_2]$ compared to [complex], and in acid solutions, undissociated H_2O_2 molecules and protonated complex A^{2+} are prevailing species. According to Eq. (10) at constant $[H^+]$, a plot of k_{obs} vs. $[H_2O_2]$ should be a straight line as obtained experimentally. The slope k_2 of these plots is found in the order of magnitude as that value of $(1 + k_4)K_1k_3[H^+]$, the slope in the derived Eq. (10). The positive intercept observed in these plots can be labeled k_1 and explained as due to the rate constant of the slow aquation at pH ≈ 3 of carrying out kinetic run (Table 3). The plot of k_{obs} vs. $[H^+]$, within the pH range 1.5–3 at constant $[H_2O_2]$, gave a straight line with a positive intercept.

Again, in the equimolar ratio, the general rate equation is

$$\frac{-d[complex]}{dt} = K_1k_3(1 + k_4)[H^+][H_2O_2][A]_T. \quad (12)$$

The general second-order rate law under these conditions is

$$\frac{-d[complex]}{dt} = k'_{obs}[H_2O_2]_T[A]_T. \quad (13)$$

Thus, k'_{obs} can be derived as

$$k'_{obs} = (1 + k_4)K_1k_3[H^+]. \quad (14)$$

The observed decrease in pH during the kinetic run from 2.3 at the beginning to 1.8 at the end of each run, suggests the liberation of the free protons as in step (IV) of the mechanism and the formation of the dissociation products in the last step (VI).

H_2O_2 has not been affected by buffer alone of pH ≈ 2.2, in which all kinetic runs were executed. It keeps constant its concentration in the buffer solution within a time of 5 h, the maximum period for a kinetic run. The intercepts, k_1 in the plots of k_{obs} vs. $[H_2O_2]$ confirm that these values are due to minor aquation of the azo complex in the aqueous medium. The characteristic band of the azo complex at 500 nm never alters and slightly decreases (~20%) in the old solution compared with the same band in the freshly prepared solution of the complex. It is worthwhile to report that azo ligands investigated are more labile against H_2O_2 than their chelates with Fe(II). This supports the proposal mechanism that the oxidation of Fe(II) to Fe(III) via inner-sphere electron transfer, enhances the subsequent degradation of the azo ligand, cf. steps (V) and (VI). This result agrees with the previous reports in the literature [32].

Table 3 shows second-order rate constants and activation parameters for representative complexes. The data indicate high stabilities leading to low reactivities against H_2O_2, and thus to large values of activation energies and to low frequency factors which are in agreement with the low values of the rate constants k_{obs}. These results support that the reaction follows an association mechanism. Negative entropies of activation and low frequency factors would support the formation of peroxo-intermediate complex and inner-sphere electron transfer mechanism [33–36].

The relative decrease in the observed rate constants (k_s/k_w), in the presence of methanol cosolvent, increases with increasing the degree of hydrophilicity of the complexes, cf. Fig. 8. Based on these relative decrease in reactivities k_s and k_w in the presence and absence of methanol in the aqueous solution respectively, cf. Fig. 8, it would be deduced the descending order of the hydrophilicity of the complexes, as follows

MimA > MphA > MinA> EinA > EphA > Eima > EprA.

The latter sequence based on the relative decrease in reactivity in aqua-methanol binary mixtures is more consistent with the structure of the investigated ligands. There is a paradox in the position of EprA, in the respective hydrophilicities derived from the different methods of the relative solubilities [18] and the relative reactivities in the aqueous solutions and in aqua–methanol binary mixtures [37]. This would be explained due to the presence of donor groups on both sides of the ligand molecule which reduce the mesomeric shift within the molecule, thus enhance the reactivity of the complex against H_2O_2. If some disagreement emerges in hydrophilicity order expected in the two different methods, this may be due to the dependency of the solubility method on the accuracy of ε_{max},

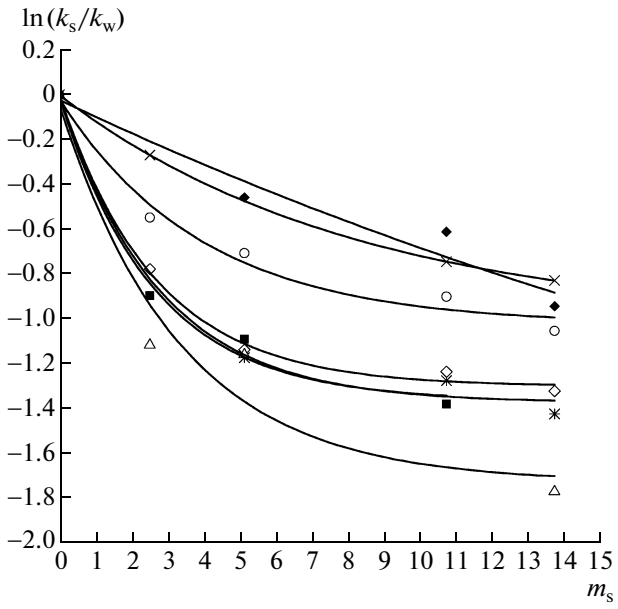

Fig. 8. Plot of $\ln(k_s/k_w)$, the relative reactivities in the aqueous containing methanol (k_s) and in methanol free aqueous solutions (k_w) for the reaction of all complexes with H_2O_2 vs. the molality (m_s) of MeOH in binary aqua-methanolic mixtures, at [complex] = 1×10^{-4}, [H_2O_2] = 0.30 M, I = 0.10 mol dm^{-3}, pH 2 and 298 K. ■, MphA; ○, EphA; *, MinA; ◇, EinA; △, MimA; ×, EimA; ◆, EprA.

the molar absorptivity, measurements for the complexes.

It is interesting here that, CH_2 spacer in all the complexes attached to the amino acid moiety, has blocked the effects of substituents R on this side of the ligand molecule. This has been observed in Table 3, that the rate constants have not altered remarkably with changing the amino acid moiety. Similar observation has been reported before [38] by our working group.

Kinetics and mechanism of the reaction of some Fe(II)–azo amino acid complexes with H_2O_2 were investigated spectrophotometrically. Following vital conclusions were recognized.

(1) The formation of intraperoxo Fe(II)–azo amino acid intermediate complex, at λ_{max} = 500 nm, is too rapid to follow in the presence of very large excess in [H_2O_2] ca. 3×10^{-3} mol dm^{-3} compared with [complex] ca. 1×10^{-4} mol dm^{-3}. The reaction of growing intraperoxo-intermediate follows first-order kinetics under these conditions.

(2) Novel spectrophotometric evidence for growing intraperoxo Fe(II)-azo amino acid complex equimolar mixing ratio of [complex] : [H_2O_2].

(3) The slow decomposition of the peroxo intermediate, in parallel with its second-order formation kinetics would exert a barrier against the precipitation of the intraperoxo Fe(II)-azo amino acid complex intermediate. It would be an ion-pair formation between the complex cation and the peroxo anion in these equimolar solutions.

(4) pH profiles show an azo/azonium equilibrium and reactivity peaks at pH 1.8–2.3. These reactivity peaks would be due to the full protonation of *N*,*N*-dialkylamino group which retards the intramolecular CT.

(5) The rate was assumed to be

$$\frac{-\mathrm{d}[\text{complex}]}{\mathrm{d}t} = \frac{-\mathrm{d}[\text{peroxo-Int}]}{\mathrm{d}t} = k_{obs}[\text{complex}],$$

where $k_{obs} = k_1 + k_2[H_2O_2]$.

(6) A mechanism was proposed involving a composite rate determining step as substitution of one H_2O molecule with peroxo in the parent complex and then oxidation *via* intraelectron transfer.

(7) Activation parameters curve evaluated by least squares of Arrhenius and Eyring plots and discussed. High negative entropy of activation assumes and evidence against the release of carboxylate by peroxide in the azo amino acid ligand.

(8) The relative decrease (k_s/k_w) in the observed rate constant, in the presence and absence of methanol, increases with increasing the degree of hydrophilicity of the reacted complexes as follows, MimA > MphA > MinA > EinA > EphA > EimA > EprA. Paradox in EprA position in the respective hydrophilicities has been assumed as due to the presence of the donor groups on both sides of the ligand molecule whereby reducing mesomeric shift and thus enhancing reactivity of the complex towards H_2O_2.

(9) It is interesting that, the methylene spacer attached to the amino acid screened the effects of the substituent on this side of the ligand molecule.

REFERENCES

1. Brausam, A. and Van Eldik, R., *Inorg. Chem.*, 2004, vol. 43, p. 5351.
2. Jantschko, W., Furtmuller, P.G., Zederbauer, M., Lanz, M., Jakopitsch, C., and Obinger, C., *Biochem. Biophys. Res. Commun.*, 2003, vol. 312, no. 2, p. 292.
3. Cyfert, M., *Inorg. Chim. Acta*, 1985, vol. 98, p. 25.
4. Koppenol, W.H., *J. Free Rad. Biol. Med.*, 1985, vol. 1, no. 4, p. 281.
5. Rahhal, S. and Richter, H.W., *J. Am. Chem. Soc.*, 1988, vol. 110, p. 3126.
6. Lu, Ming-C., Chen, Jong-N., and Chang, Cheu-P., *J. Hazard. Mater.*, 1999, vol. 65, no. 3, p. 277.
7. Dunford, H.B., *J. Free Rad. Biol. Med.*, 1987, vol. 3, no. 6, p. 405.
8. Truong, G.L., De Laat, J.D., and Legube, B., *Water Res.*, 2004, vol. 38, no. 9, p. 2384.
9. Blandamer, M.J., Burgess, J., Philip, P.D., and Robert, I.H., *J. Chem. Soc., Dalton Trans.*, 1980, p. 2442.
10. Burgess, J. and Shraydeh, B., *Polyhedron*, 1992, vol. 11, no. 16, p. 2015.

11. Salem, I.A., *Appl. Catal.*, 2000, vol. 28, nos. 3–4, p. 153.
12. Goszczynski, S., Paszczynski, A., Pasi-Grigsby, M.B., Crawford, R.L., and Crawford, D.L., *J. Bacteriol.*, 1994, vol. 176, p. 1339.
13. Tarin, P. and Blano, M., *Analyst*, 1988, vol. 113, no. 3, p. 433.
14. Chivukula, M., Spadaro, J.T., and Renganathan, V., *Biochemistry*, 1995, vol. 34, p. 7765.
15. Jones, P. and Wilson, I., *Met. Ions Biol. Syst.*, 1978, vol. 7, p. 185.
16. Oakes, J. and Gratton, P., *J. Chem. Soc., Perkin Trans. 2*, 1998, vol. 9, p. 1857.
17. Oakes, J. and Gratton, P., *J. Chem. Soc., Perkin Trans. 2*, 1998, vol. 10, p. 2201.
18. Shaker, A.M. and Adam, M.S., *Synth. React. Inorg. Met.-Org. Chem.*, 2003, vol. 33, no. 6, p. 1081.
19. Krumholz, P., *Inorg. Chem.*, 1965, vol. 4, p. 609.
20. Blandamer, M.J., Burgess, J., Clark, B., Duce, P.P., Hakin, A.W., Gosal, N., Radulovic, S., Guardado, P., Sanchez, F., Hubbard, C.D., and Abu-Gharib, E.A., *J. Chem. Soc., Faraday Trans. 1*, 1986, vol. 82, p. 1471.
21. Blandamer, M.J., Burgess, J., Elvidge, D.L., Guardado, P., Hakin, A.W., Prouse, L.G.S., Radulovic, S., and Russell, D.R., *Trans. Met. Chem.*, 1991, vol. 16, p. 82.
22. Shaker, A.M., Awad, A.M., and Nassr, L.A.E., *Int. J. Chem. Kinet.*, 2002, vol. 34, p. 595.
23. Rizkalla, E.N., Anis, S.S., and Khalil, L.H., *Polyhedron*, 1987, vol. 6, no. 3, p. 403.
24. Anis, S.S., Mansour, M.A., and Khalil, L.H., *J. Chem. Phys.*, 1991, vol. 88, p. 643.
25. Anis, S.S. and Mansour, M.A., *Int. J. Chem. Kinet.*, 1991, vol. 23, p. 389.
26. Beck, M.T., *Chemistry of Complex Equilibria*, London: Van Nostrand Reinhold, 1972, p. 162.
27. Ogata, Y. and Takagi, Y., *J. Chem. Soc., Dalton Trans.*, 1958, vol. 80, p. 3591.
28. Zhou, Y.M., Leng, W.N., Xu, Q.H., and Liu, J.Z., *Polymer*, 2001, vol. 42, p. 9253.
29. Francis, K.C., Cummins, D., and Oakes, J., *J. Chem. Soc., Dalton Trans.*, 1985, p. 493.
30. Nango, M., Iwasaki, T., Takeuchi, Y., Kurono, Y., Tokuda, J., and Oura, R., *Langmuir*, 1998, vol. 14, no. 12, p. 3272.
31. Shaker, A.M., *J. Colloids Interface Sci.*, 2001, vol. 233, p. 197.
32. Pignatello, J.J., MacKay A.A, *Helv. Chim. Acta*, 2001, vol. 84, p. 2589.
33. Stasko, A., Erentova, K., Rapta, P., Nuyken, O., and Voit, B., *Magn. Reson. Chem.*, 1998, vol. 36, p. 13.
34. Stewart, R., *J. Am. Chem. Soc.*, 1957, vol. 79, p. 3057; Stewart, R. and Maden, R.V., *Discuss. Faraday Soc.*, 1960, p. 211.
35. Stewart, R. and Mocek, M.M., *Can. J. Chem.*, 1963, vol. 41, p. 1160.
36. Stasko, A., Erentova, K., Rapta, P., Nuyken, O., and Voit, B., *Magn. Reson. Chem.*, 1998, vol. 36, p. 13.
37. Shaker, A.M., Zwaik, A.A.S., and Adam, M.S.S., *Global J. Phys. Chem.* (in press).
38. Alshehri, S., Burgess, J., and Shaker, A.M., *Transition Met. Chem.*, 1998, vol. 23, p. 689.